ASTRONOMY & ASTROPHYSICS
SUPPLEMENT SERIES

NOVEMBER II **1999**, PAGE 99

Astron. Astrophys. Suppl. Ser. **140**, 99–105 (1999)

Analysis of CMB maps with 2D wavelets

J.L. Sanz[1], **R.B. Barreiro**[1,2], **L. Cayón**[1], **E. Martínez-González**[1], **G.A. Ruiz**[3], **F.J. Díaz**[3], **F. Argüeso**[4], **J. Silk**[5], **and L. Toffolatti**[6,7]

[1] Instituto de Física de Cantabria, Fac. Ciencias, Avda. de los Castros s/n, 39005 Santander, Spain
[2] Dpto. Física Moderna, Universidad de Cantabria, Avda. de los Castros s/n, 39005 Santander, Spain
[3] Dpto. de Electrónica y Computadores, Universidad de Cantabria, Avda. de los Castros s/n, 39005 Santander, Spain
[4] Dpto. Matemáticas, Universidad de Oviedo, c/ Calvo Sotelo s/n, 33007 Oviedo, Spain
[5] Astronomy Dept. & Center for Particle Astrophysics, University of California, 601 Campbell Hall, Berkeley, CA 94720, U.S.A.
[6] Dpto. de Física, Universidad de Oviedo, c/ Calvo Sotelo s/n, 33007 Oviedo, Spain
[7] Osservatorio Astronomico di Padova, vicolo dell'osservatorio n5, 35122 Padova, Italy

Received March 11; accepted August 26, 1999

Abstract. We consider the 2D wavelet transform with two scales to study sky maps of temperature anisotropies in the cosmic microwave background radiation (CMB). We apply this technique to simulated maps of small sky patches of size $12.8^\circ \times 12.8^\circ$ and $1.5' \times 1.5'$ pixels. The relation to the standard approach, based on the $C_l's$, is established through the introduction of the scalogram. We consider temperature fluctuations derived from standard, open and flat-Λ Cold Dark Matter (CDM) models. We analyze CMB anisotropies maps plus uncorrelated Gaussian noise (uniform and non-uniform) at different S/N levels. We explore in detail the denoising of such maps and compare the results with other techniques already proposed in the literature. Wavelet methods provide a good reconstruction of the image and power spectrum. Moreover, they are faster than previously proposed methods.

Key words: cosmology: cosmic microwave background — methods: data analysis

1. Introduction

Future Cosmic Microwave Background (CMB) experiments will provide high resolution sky maps covering a wide range of frequencies. In addition to the cosmological CMB signal those maps will contain instrumental noise and contributions from Galactic and extragalactic foregrounds. The denoising of these maps as well as the separation of the different components from the CMB signal are the most challenging problems for CMB cosmology. The final goal would be to reconstruct CMB maps trying not to loose structural details as well as to recover the radiation power spectrum with the minimum error. In a first approach to these problems we present in this paper a denoising technique based on wavelets. Previously there have been other works based in the use of Wiener filter (Tegmark & Efstathiou 1996) and Maximum Entropy Methods (Hobson et al. 1998, 1999). The use of denoising methods based on wavelets have certain advantages as providing information of the contribution of different scales, being computationally faster ($0(N)$) and not requiring iterative processes. The analysis of discrete 2-dimensional images with wavelets can be performed following different approaches. The two computationally faster algorithms are the ones based on Multiresolution analysis (Mallat 1989) and on 2D wavelet analysis (Lemarié & Meyer 1986), using tensor products of one dimensional wavelets. A study of denoising of CMB maps using the former method has been presented in Sanz et al. (1999). This method is based on a single scale and three "details" at each resolution level. The 2-D wavelet method used in this work is based on two scales, providing therefore more information on different resolutions (defined by the product of the two scales) than the Multiresolution one. Moreover this technique is adapted to separable wavelets. On the other hand, an analysis of denoising using spherical wavelets has been recently carried out by Tenorio et al. (1999).

The paper is organized as follows. In Sect. 2 we present some basic ideas about the continuous 2D wavelet transform. We apply 2-D wavelets to the analysis of discrete 2D CMB anisotropy maps of small sky patches in Sect. 3 and the conclusions are presented in Sect. 4.

Send offprint requests to: L. Cayón

2. 2D continuous wavelet transform

This section is dedicated to present the continuous form of the 2D wavelet approach we are later using to analyse discrete CMB maps. As a difference with the multiresolution approach used in Sanz et al. (1999) the 2D wavelet method provides information on many more resolution elements than the former method. Moreover, this property is crucial for performing an efficient linear denoising preserving the Gaussianity of the underlying CMB field (as will be discussed in Sect. 3.2).

The continuous wavelet transform of a 2D signal $f(x_1, x_2)$ is defined as

$$w(R_1, R_2, b_1, b_2) = \int \mathrm{d}x_1\, \mathrm{d}x_2\, f(x_1, x_2) \times \Psi(R_1, R_2, b_1, b_2; x_1, x_2)\,, \quad (1)$$

$$\Psi(R_1, R_2, b_1, b_2; x_1, x_2) = \frac{1}{\sqrt{|R_1 R_2|}} \times \psi\left(\frac{x_1 - b_1}{R_1}, \frac{x_2 - b_2}{R_2}\right), \quad (2)$$

where $w(R_1, R_2, b_1, b_2)$ is the wavelet coefficient associated to the scales R_1 and R_2 at the point with coordinates b_1 and b_2. The limits in the double integral are $-\infty$ and ∞ for the two variables. ψ is the wavelet "mother" function that satisfies the constraints

$$\int \mathrm{d}x_1\, \mathrm{d}x_2\, \psi = 0, \quad \int \mathrm{d}x_1\, \mathrm{d}x_2\, \psi^2 = 1, \quad (3)$$

and the "admissibility" condition (that allows to reconstruct the function f), i.e. there exists the integral

$$C_\psi \equiv (2\pi)^2 \int \mathrm{d}k_1\, \mathrm{d}k_2 \frac{|\hat{\psi}(k_1, k_2)|^2}{|k_1\, k_2|}, \quad (4)$$

where $\hat{\psi}(k_1, k_2)$ represents the 2D Fourier transform of ψ and $||$ denotes the modulus of the complex number.

A reconstruction of the image can be achieved with the inversion formula

$$f(x_1, x_2) = \frac{1}{C_\psi} \int \frac{\mathrm{d}R_1\, \mathrm{d}R_2}{|R_1\, R_2|^2}\, \mathrm{d}b_1\, \mathrm{d}b_2\, w(R_1, R_2, b_1, b_2) \times \Psi(R_1, R_2, b_1, b_2; x_1, x_2)\,. \quad (5)$$

Next, let us introduce the scalogram of a 2D signal

$$\sigma_{\mathrm{w}}^2(R_1, R_2) \equiv \langle w^2(R_1, R_2, b_1, b_2) \rangle \quad (6)$$

where $\langle\rangle$ means the average value calculated on the image.

Hereinafter, we shall consider 2D wavelets that are separable, i.e. $\psi(x_1, x_2) = \psi(x_1)\psi(x_2)$. In this case, $|\hat{\psi}(k_1, k_2)|^2 = |\hat{\psi}(k_1)|^2 |\hat{\psi}(k_2)|^2$. In particular, we are interested in the Haar, the Mexican Hat and the Daubechies 2D-transforms that can be generated in terms of the corresponding 1D wavelets. For the Haar case, we find

$$|\hat{\psi}(k)|^2 = \frac{8}{\pi k^2} \sin^4\left(\frac{k}{4}\right), \quad (7)$$

with an absolute maximum at $k \simeq 4.7$, whereas for the Mexican Hat

$$|\hat{\psi}(k)|^2 = \frac{4}{3\pi^{1/2}} k^4 \mathrm{e}^{-k^2}, \quad (8)$$

with a single peak at $k = \sqrt{2}$. The corresponding formulae for the Daubechies wavelets of order N can be found in Ogden (1997). The last wavelets form an orthonormal basis with compact support, increasing regularity with N and vanishing moments up to order $N - 1$.

Just as an illustration we would like to present the scalogram for a CMB signal generated in a Standard Cold Dark Matter (SCDM) model. Let us assume that the image corresponds to a realization of a random field whose 2-point correlation function is homogeneous and isotropic: $\xi(r)$, $r^2 \equiv x_1^2 + x_2^2$. This is equivalent to assume that the Fourier components $\hat{f}(k_1, k_2)$ satisfy

$$\langle \hat{f}(k_1, k_2)\, \hat{f}^*(k_1', k_2') \rangle = P(k) \delta(k_1 - k_1') \delta(k_2 - k_2'), \quad (9)$$

where $P(k)$, $k^2 \equiv k_1^2 + k_2^2$, is the standard Fourier power spectrum and $\langle\rangle$ means average value over realizations of the field (the ergodicity of the field is assumed). So, taking average values and using Eqs. (1) and (6), one obtains the variance $\sigma_{\mathrm{w}}^2(R_1, R_2)$ of the wavelet coefficients or scalogram

$$\sigma_{\mathrm{w}}^2(R_1, R_2) = R_1 R_2 \int \mathrm{d}k_1\, \mathrm{d}k_2\, P(k) |\hat{\psi}(k_1 R_1, k_2 R_2)|^2. \quad (10)$$

For 2D white noise, i.e. $P(k) =$ constant, one gets that the scalogram, σ_{w}^2, is constant at any scale.

On the other hand, if the field f represents the temperature anisotropy of the CMB, $\frac{\Delta T}{T}$, one can obtain

$$\left\langle \left(\frac{\Delta T}{T}\right)^2 \right\rangle = \frac{1}{C_\psi} \int \mathrm{d}R_1\, \mathrm{d}R_2 \frac{\sigma_{\mathrm{w}}^2(R_1, R_2)}{R_1^2 R_2^2}. \quad (11)$$

From the previous equation, $\sigma_{\mathrm{w}}^2 / C_\psi R_1 R_2$ represents the power per logarithmic scale. We remark that taking into account the homogeneity and isotropy of the field, the 2-scale dependence of the scalogram is redundant in this case. A more appropriate treatment in this continuous example would be one based on isotropic wavelets defined in terms of a single scale.

In the top panel of Fig. 1 we have represented the scalogram against the two scales R_1 and R_2 for SCDM using the Haar transform. The qualitative behaviour for the other transforms is similar. In the bottom panel we compare the scalogram along the diagonal for standard, open ($\Omega = 0.3$) and a flat-Λ ($\Omega = 0.3, \lambda = 0.7$) CDM models using the Haar and the Mexican Hat transforms. The qualitative behaviour for the two transforms is similar: there is a plateau for $R > 1^\circ$ and a maximum dependent on Ω, corresponding to the first Doppler peak. Other secondary maxima appearing in the figure are related to the secondary peaks in the standard C_ℓ radiation power spectrum (the C_ℓ is given by $C_\ell \simeq P(k \simeq \ell)$). Therefore, the position and amplitude of the maxima that appear in the scalogram is model dependent, being this quantity tightly related to the C_ℓ's.

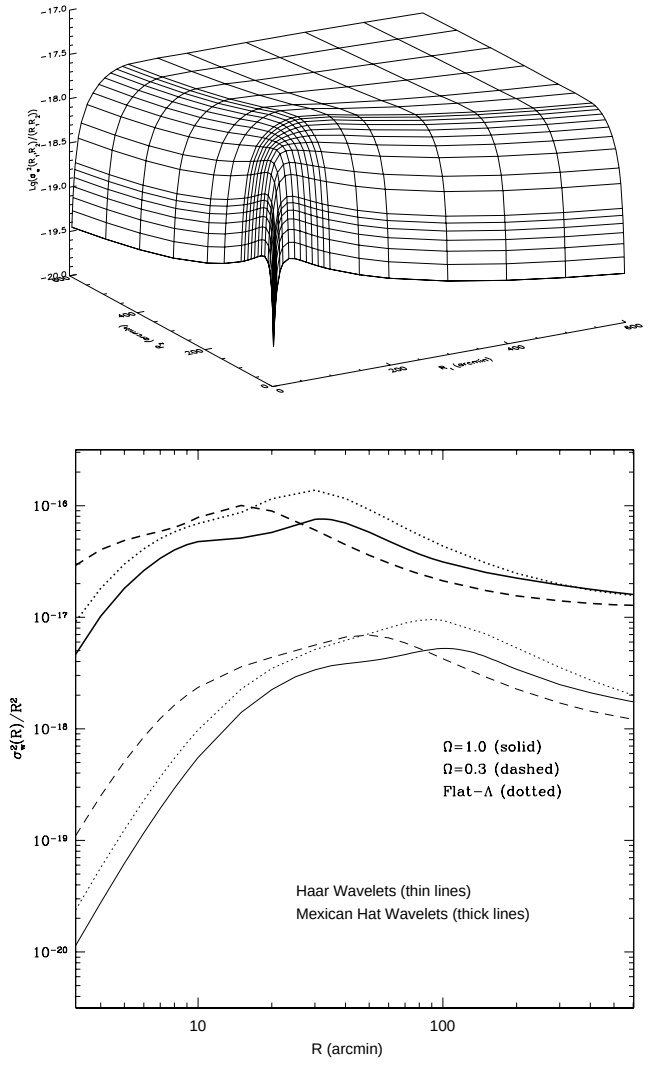

Fig. 1. Top: scalogram for a SCDM model using the Haar wavelet. Bottom: scalogram along the diagonal, i.e., $R_1 = R_2$, for the SCDM (solid line), open CDM (dashed line) and flat-Λ CDM (dotted line) models using the Haar (thin lines, bottom of the panel) and Mexican Hat (thick lines, top of the panel) wavelets

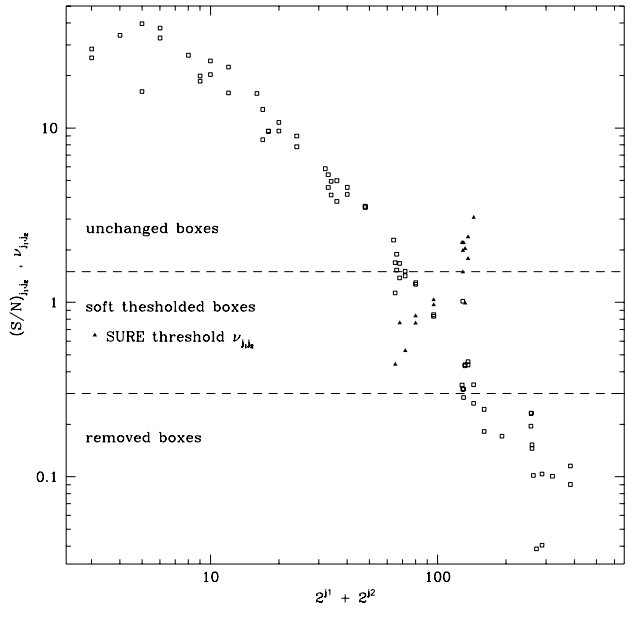

Fig. 2. S/N ratio (open squares) in each box for a CMB map (SCDM model) with uniform noise at the level $S/N = 1$ using Daubechies 4. The three regions of the plot show the boxes that are kept unchanged ($S/N \geq 1.5$), removed ($S/N < 0.3$) or treated with a soft thresholding technique (boxes in between). The soft thresholds (solid triangles) estimated using SURE are also plotted for the thresholded boxes

3. Denoising of CMB maps

3.1. 2D wavelet method on a grid

In general for a grid of $2^n \times 2^n$ pixels, a discretization of the parameters of the form: $R_1 = 2^{n-j_1}, b_1 = 2^{n-j_1} l_1, R_2 = 2^{n-j_2}, b_2 = 2^{n-j_2} l_2$ for integer-valued j and l allows to introduce the 2D discrete wavelet function

$$\Psi_{j_1,j_2,l_1,l_2}(x_1,x_2) = 2^{(j_1+j_2)/2-n}\psi(2^{j_1-n}x_1 - l_1) \times\psi(2^{j_2-n}x_2 - l_2)\,, \quad (12)$$

where j_i and l_i denote the dilation and the translation indexes, respectively, satisfying $0 \leq j_1, j_2 \leq n-1, 0 \leq l_1 \leq 2^{j_1} - 1, 0 \leq l_2 \leq 2^{j_2} - 1$. The resolution level is defined by $j = \frac{j_1+j_2}{2}$, corresponding to $R \equiv \sqrt{R_1 R_2} = 2^{n-j}$. We also introduce a scaling function ϕ that allows to define a complete basis to reconstruct discrete images,

$$\Phi_{0,0,0,0}(x_1,x_2) = 2^{-n}\phi(2^{-n}x_1)\phi(2^{-n}x_2), \quad (13)$$

$$\Gamma^{\rm H}_{0,j_2,0,l_2}(x_1,x_2) = 2^{j_2/2-n}\phi(2^{-n}x_1)\psi(2^{j_2-n}x_2 - l_2), \quad (14)$$

$$\Gamma^{\rm V}_{j_1,0,l_1,0}(x_1,x_2) = 2^{j_1/2-n}\psi(2^{j_1-n}x_1 - l_1)\phi(2^{-n}x_2). \quad (15)$$

We will consider orthonormal discrete bases as the Haar and Daubechies ones. Denoting by Λ any of the previous functions, the orthonormality condition reads:

$$(\Lambda_{j_1,j_2,l_1,l_2}, \Lambda_{j_1',j_2',l_1',l_2'}) = \delta_{j_1 j_1'}\delta_{j_2 j_2'}\delta_{l_1 l_1'}\delta_{l_2 l_2'}, \quad (16)$$

where (f,g) denotes the scalar product of two functions in $L^2(R^2)$.

The wavelet coefficients are now defined by

$$w_{j_1,j_2,l_1,l_2} = \int {\rm d}x_1\, {\rm d}x_2\, f(x_1,x_2)\Lambda_{j_1,j_2,l_1,l_2}. \quad (17)$$

The image is reconstructed using the following expression:

$$f(x_1,x_2) = \sum_{j_1 j_2 l_1 l_2} w_{j_1,j_2,l_1,l_2}\Lambda_{j_1,j_2,l_1,l_2}(x_1,x_2). \quad (18)$$

A representation of the wavelet coefficients can be done by a square that contains small squares and rectangles associated to different levels of resolution. The first level, representing high-resolution, is $j_1 = j_2 = 8$ (i.e. $j = 8$)

that contains 65536 wavelet coefficients (each one constructed with $2 \times 2 = 4$ pixels for the Haar transform). The second level of resolution contains two boxes: $j_1 = 8, j_2 = 7$ and $j_1 = 7, j_2 = 8$ (i.e. $j = 7.5$) with a total of 2×32768 wavelet coefficients (each one constructed with $2^2 \times 2 = 2 \times 2^2 = 8$ pixels for the Haar transform). The levels with $j_1 = 0$ (or $j_2 = 0$) contain both contributions from wavelet-wavelet and scaling-wavelet (or wavelet-scaling). Finally, the lower level of resolution is $j_1 = j_2 = 0$ (i.e. $j = 0$) and contains four contributions: wavelet-wavelet, wavelet-scaling, scaling-wavelet and scaling-scaling (this last one is proportional to the average value of the image for the Haar transform).

3.2. Reconstruction of CMB maps and radiation power spectra

In the present work we have considered simulated maps of size $12.8^\circ \times 12.8^\circ$ square degrees, pixel $1.5' \times 1.5'$ and filtered with a $4.5'$ FWHM Gaussian beam for a standard CDM model ($\Omega = 1$). We have included non-correlated Gaussian noise at different levels (S/N per pixel between 0.7 and 3 at the pixel scale), considering uniform and non-uniform noise. This last case is introduced to account for the non-uniform sampling of satellite observations. As an extreme case we have simulated a noise map with two different regions, one with $S/N = 3$ (approximately one quarter of the map) and a second one with $S/N = 0.7$.

The purpose of the denosing of CMB maps is to reconstruct the original signal map as well as the radiation power spectrum C_ℓ.

Wavelet decompositions are performed with the package *2D-W* developed by our group. The procedure uses two scales, $R_1 = 2^{n-j_1}$, $R_2 = 2^{n-j_2}$, $n = 9$ in our case. High values of $j = (j_1 + j_2)/2$ mean high resolution, i.e., small scales. We distribute the coefficients w_{j_1,j_2,l_1,l_2} in boxes corresponding to a couple (j_1, j_2), having a total of 81 boxes. The coefficients related to the scaling function are not included in the analysis and they are left untouched. To perform denoising, the basic operation is the comparison between the wavelet coefficients dispersion of the signal in each box with the one of the noise. The Gaussian white noise gives the same contribution in all boxes. Since the signal is negligible at the highest resolutions, the noise dispersion can be directly estimated from the map. Therefore, the signal dispersion can also be estimated for each box.

In Fig. 2, we plot the S/N ratio (defined in terms of the wavelet coefficients dispersions of signal and noise) for each box for a CMB simulation with $S/N = 1$ in real space.

For the case of uniform noise, all boxes where the signal dominates ($S/N \geq 1.5$) are kept untouched, whereas those with a high level of noise ($S/N < 0.3$) are removed. On the other hand, the boxes in between are treated with a soft thresholding technique. Given a threshold ν in terms of the noise coefficients dispersion (σ_n), the coefficients $|w| > \nu\sigma_n$ are rescaled as $w' = w \pm \nu\sigma_n$ (where the $+$, $-$ signs correspond to negative and positive values of w respectively), whereas the remaining coefficients are set to zero. The threshold ν for each box is chosen using the SURE method (Donoho & Johnstone 1995). The threshold is obtained by minimization of an unbiased estimate of the expected mean squared error of the estimation of the signal wavelet coefficients (see for instance Ogden 1997). In Fig. 2, the thresholds obtained with the SURE technique are plotted for a CMB map with $S/N = 1$. As expected, lower S/N levels are treated with higher thresholds, i.e., more coefficients are removed. Changing the range of S/N where the soft technique is applied (providing is around $S/N = 1$), does not appreciably change these results. We have used Daubechies 4 but we obtain little or no variations if we adopt higher order Daubechies wavelets. However, the Haar transform gives worse results. Table 1 shows the error in the map reconstructions for different S/N ratios with Gaussian uniform noise. The error improvement achieved with the denoising technique applied goes from factors of 3 to 5 for $S/N = 3 - 0.7$. The four top panels of Fig. 3 show CMB maps with only signal (SCDM), signal plus noise with a $S/N = 1$, the reconstructed map using wavelets and the residual one.

Table 1. Reconstruction errors (%)

S/N	SURE	linear
0.7	27.4	29.4
1.0	21.7	23.4
2.0	13.3	14.4
3.0	10.0	11.1
N.U.	24.3	–

Regarding non-uniform (N.U.) noise, wavelet techniques allow us to treat each location in the image separately. At each fixed location and fixed (j_1, j_2) we calculate the dispersion of the corresponding noise wavelet coefficient from 500 simulations of our non-uniform noise. Since we consider non-uniform noise that is uncorrelated, the average noise dispersion is the same for all the boxes, as in the uniform noise case. Therefore, we can get again the dispersion of the signal for each (j_1, j_2) pair as well as the S/N ratio for each coefficient. Those coefficients with S/N ratio in the considered range ($0.3 \leq S/N < 1.5$) are treated with a soft thresholding technique, whereas the rest are either kept or removed depending on their S/N ratio. Since in presence of non-uniform noise, we cannot use the SURE technique to estimate the optimal threshold ν (as far as we know, work is in progress to define a general threshold in the case of non-uniform noise, Von Sachs & McGibbon 1999), we choose for all the thresholded coefficients $\nu = 1$. This threshold is defined with respect

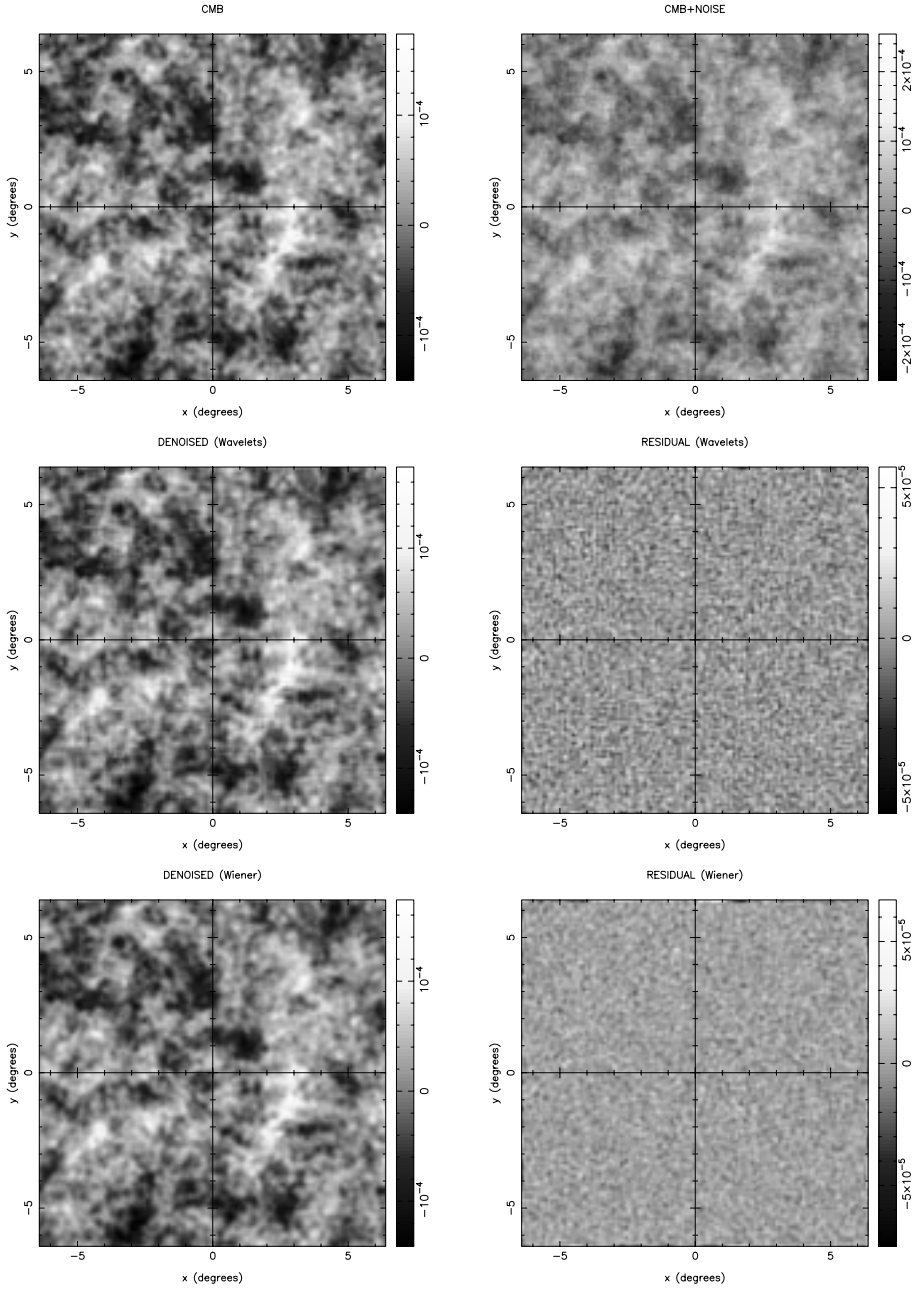

Fig. 3. Simulated map of the cosmological signal for the SCDM model (top left), signal plus uniform noise with $S/N = 1$ (top right), denoised map using wavelets (middle left) and residual map obtained from the CMB signal map minus the denoised one (middle right). For comparison the denoised map using Wiener filter (bottom left) is also shown together with the corresponding residuals (bottom right)

to the noise dispersion in each particular coefficient. We have chosen this value of ν because it gives a good reconstruction when comparing with the original map, but the results are not very sensitive to the choice of a different threshold in the range $\nu = 0.8 - 2.0$. In Table 1 we present the error of the reconstructed map in the presence of non-uniform noise as considered in this work.

Regarding the power spectrum, C_ℓ, the denoising method performs very well. Figures 4 and 5 show the reconstructed spectrum and the relative error for $\ell < 2000$ for different S/N ratios (the power spectrum is obtained in the usual way, averaging over the Fourier modes of the considered map at each k). The relative error is $\lesssim 20\%$ for $\ell < 1700$ in all the considered cases except for the map with $S/N = 0.7$. In this last case the error increases to $\lesssim 30\%$ for the same range of $\ell's$.

Finally, we have looked for possible non-Gaussian features introduced by the non-linearity of the soft thresholding technique. We have compared the

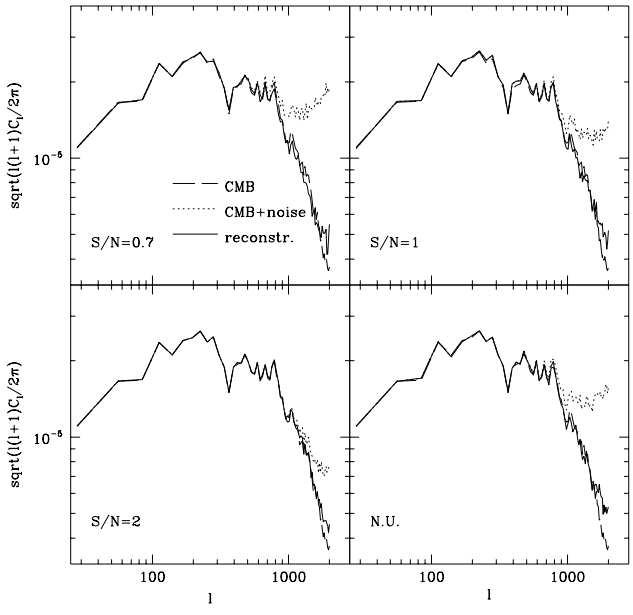

Fig. 4. Power spectrum of the original CMB (dashed line), CMB plus noise (dotted line) and reconstructed maps using wavelets (solid line) for different levels of noise. Top left panel corresponds to $S/N = 0.7$, top-right to $S/N = 1$, bottom-left to $S/N = 2$ and bottom-right to non-uniform noise (the non-uniform noise map consists in two regions of different S/N ratio; approximately one quarter of the map is at the level of $S/N = 3$ and the rest at $S/N = 0.7$)

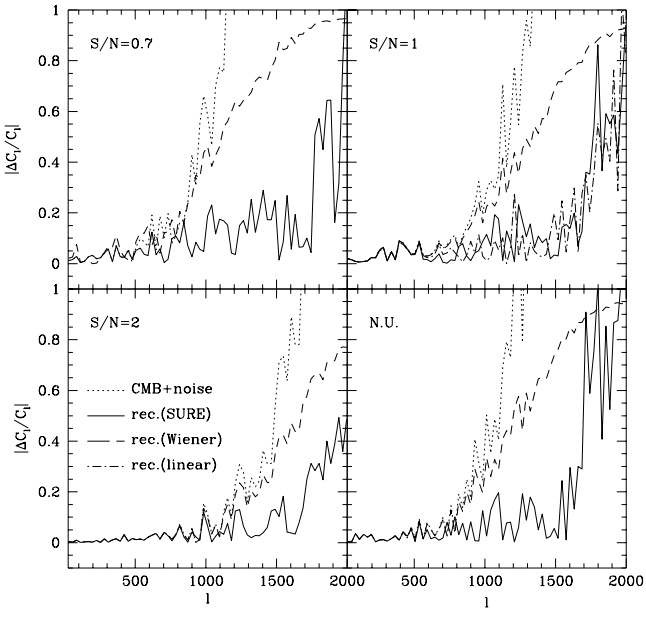

Fig. 5. Absolute value of the relative errors of the CMB power spectrum obtained from signal plus noise maps (dotted line), wavelet denoised maps using the SURE thresholding technique (solid line), Wiener denoised maps (dashed line) and wavelet denoised map using a linear method, only on the top-right panel (dot-dashed line). Top-left panel corresponds to $S/N = 0.7$, top-right to $S/N = 1$, bottom-left to $S/N = 2$ and bottom-right to non-uniform noise

probability density function of the original and the reconstructed maps using a Kolmogorov-Smirnov test. Both distributions are compatible at similar or higher levels than the original map and the corresponding linear reconstruction obtained with the Wiener Filter technique. Moreover, not significant change is observed in the skewness and kurtosis of the original and reconstructed maps. However, the application of soft thresholding to the wavelet coefficients at a certain level, which are Gaussian distributed for a Gaussian temperature field, clearly changes their distribution by removing all coefficients whose absolute values are below the imposed threshold and shifting the remaining ones by that threshold. Therefore, this technique is introducing a certain level of non-Gaussianity that will depend on the threshold imposed and that should be taken into account when analysing the data. If we are mainly concern about preserving the Gaussian character of the reconstructed image, denoising with wavelet techniques is still possible. Instead of using a soft thresholding technique, we can apply a linear denoising method in wavelet space. In particular, we have removed all wavelet coefficients at boxes with $S/N < 1$ and left the rest untouched. The reconstruction errors get only slightly worse with this simple linear technique as shown in Table 1. Regarding the reconstructed power spectrum, this is at the same level than the SURE reconstruction (see top-right panel of Fig. 5) for all the considered cases. It is important to remark that the linear denoising method based on 2D wavelets performs much better than the Multiresolution one due to the larger number of boxes corresponding to the product of the 2 scales considered.

3.3. Comparison with other denoising methods

A comparison between Wiener Filter (see for instance Press et al. 1994) and wavelet techniques has also been performed. In relation to map reconstruction the error affecting the Wiener reconstructed maps is comparable to that achieved with wavelet techniques in all the considered cases. However, in order to apply Wiener filter previous knowledge of the signal power spectrum is required. In a real situation this may well not be possible. The reconstructed and residual maps using Wiener Filter are shown in Fig. 3. In addition, when using Wiener Filter, the power spectrum of the reconstructed image is clearly suppressed at high $\ell's$, giving much worse results than the wavelet technique. For comparison, we have plotted in Fig. 5 the absolute value of the relative error of the $C'_\ell s$ for the reconstructions with Wiener Filter. On the other hand, one

could recover the C_ℓ's of the original signal by subtracting from the power spectrum of the signal plus noise map the estimated power spectrum of the noise, which is constant at each ℓ. However, this method gives in general worse results than the wavelet techniques and besides cannot be used to reconstruct the image. We have also applied a Maximum Entropy Method to the maps used in this work, with the definition of entropy given by Hobson & Lasenby (1998). This method provides reconstruction errors at similar levels as the wavelet techniques. However, we remark that wavelet techniques are computationally faster $0(N)$ and simpler to apply (not requiring iterative processes) than Maximum Entropy Methods.

4. Conclusions

We have considered the 2D wavelet transform with two scales to analyse CMB maps. First of all we present the continuous approach to the 2D wavelet. A discrete analysis is performed for a finite image. In this case, a scaling function is introduced in order to define a 2D wavelet basis.

The 2D wavelet technique has been applied to denoise CMB maps for S/N ratios ranging between 0.7 and 3. We have also considered the case of non-uniform Gaussian noise. A factor between 5 and 3 is gained for the reconstructed images/original signal map in relation to the signal plus noise maps/original signal map. Regarding the $C'_\ell s$, the relative errors are below a 20% up to $\ell = 1700$ for all the cases with $S/N \geq 1$. A comparison with Wiener Filter and Maximum Entropy Method has also been performed. The later gives comparable reconstructions to the wavelet method, being however slower and more complicated to apply. Wiener Filter provides reconstructed maps with errors comparable to the wavelet technique we propose. However, unlike the wavelet method, Wiener filter requires previous knowledge of the signal power spectrum. Moreover, the $C'_\ell s$ of the denoised map obtaining by applying Wiener filter are clearly underestimated.

Finally, we would like to remark that linear wavelet denoising, which preserves Gaussianity, gives reconstruction errors similar to those obtained with the non-linear soft thresholding techniques. Moreover, linear denoising is better achieved by 2D wavelets than by the multiresolution ones discussed in Sanz et al. (1999).

Acknowledgements. This work has been supported by the DGESIC Project No. PB95-1132-C02-02, CICYT Acción Especial No. ESP98-1545-E and Comisión Conjunta Hispano-Norteamericana de Cooperación Científica y Tecnológica with Ref. 98138. RBB has been supported by a Spanish MEC fellowship. JLS acknowledges partial financial support from a Sabbatical Grant by the Spanish DGESIC. JLS, RBB and LC thank the hospitality of the Center for Particle Astrophysics and the Astronomy Department of the University of California at Berkeley. LT acknowledges partial financial support from the "Agenzia Spaziale Italiana" (ASI) and Consiglio Nazionale delle Ricerche (CNR).

References

Donoho D.L., Johnstone I.M., 1995, J. Am. Stat. Assoc. 90, 1200

Hobson M.P., Barreiro R.B., Toffolatti L., Lasenby A.N., Sanz J.L., Jones A.W., Bouchet F.R., 1999, MNRAS 306, 232

Hobson M.P., Jones A.W., Lasenby A.N., Bouchet F., 1998, MNRAS 300, 1

Hobson M.P., Lasenby A.N., 1998, MNRAS 298, 905

Lemarié P.G., Meyer Y., 1986, Rev. Mat. Ib. 2, 1

Mallat S.G., 1989, IEEE Trans. Pat. Anal. Mach. Int. 11, 674

Ogden R.T., 1997, Essential wavelets for statistical applications and data analysis. Birkhäuser, Boston

Press W.H., Teukolsky S.A., Vetterling W.T., Flannery B.P., 1994, Numerical Recipes in Fortran, Second edition. Cambridge: Cambridge University Press, p. 539

Sanz J.L., Argüeso F., Cayón L., Martínez-González E., Barreiro R.B., Toffolatti L., 1999, MNRAS (in press)

Tegmark M., Efstathiou G., 1996, MNRAS 281, 1297

Tenorio L., Jaffe A.H., Hanany S., Lineweaver C.H., 1999, MNRAS (submitted)

Von Sachs R., MacGibbon B., 1999, Scand. J. Stat. (submitted)